JOURNAL OF THERMOPHYSICS AND HEAT TRANSFER
Vol. 17, No. 1, January–March 2003

# Heat (Mass) Transfer on Effusion Plate in Impingement/Effusion Cooling Systems

Dong Ho Rhee,* Jong Hyun Choi,* and Hyung Hee Cho†
*Yonsei University, Seoul 120-749, Republic of Korea*

**The local heat/mass transfer characteristics on an inner surface of the effusion plate in an impingement/effusion cooling system have been investigated. Two perforated plates are installed in parallel position to simulate the impingement/effusion cooling system. The experiments have been conducted for three different hole arrangements, staggered, square, and hexagonal, with various gap distances of 1, 2, 4, and 6 times the effusion hole diameter. The Reynolds number based on the effusion hole diameter is fixed at $1 \times 10^4$. A naphthalene sublimation method is used to determine the local heat/mass transfer coefficients on the effusion plate. For all of the tested cases, high transfer regions are formed near the stagnation points and at the midline region of the adjacent impinging jets due to secondary vortices and flow acceleration to the effusion holes. The heat/mass transfer coefficient in the whole region increases with decreasing gap distance. The staggered hole arrangement shows the highest average heat transfer coefficient due to the largest area ratio of the effusion to the injection hole; however, the heat/mass transfer on the effusion plate is more uniform for the square and hexagonal hole arrangements because the number of injection holes is increased.**

## Nomenclature

| | | |
|---|---|---|
| $A_e$ | = | total hole area of effusion plate |
| $A_i$ | = | total hole area of injection plate |
| $D$ | = | effusion hole diameter |
| $d$ | = | injection hole diameter |
| $H$ | = | gap distance between injection and effusion plates |
| $h_m$ | = | local mass transfer coefficient |
| $K_{\text{naph}}$ | = | mass diffusion coefficient of naphthalene vapor in air |
| $N_D$ | = | number of effusion holes |
| $N_d$ | = | number of injection holes |
| $Nu$ | = | Nusselt number based on effusion hole diameter |
| $P$ | = | pitch of array holes |
| $Pr$ | = | Prandtl number |
| $Re_D$ | = | Reynolds number based on effusion hole diameter and the average velocity in the hole |
| $Re_d$ | = | Reynolds number based on injection hole diameter and the average velocity in the hole |
| $Sc$ | = | Schmidt number |
| Sh | = | Sherwood number based on effusion hole diameter, Eq. (2) |
| $\overline{\text{Sh}}$ | = | average Sherwood number |
| $x, z$ | = | distance from the center of a hole (Fig. 2) |

## Introduction

MODERN gas turbine engines are designed to be operated at high turbine inlet temperature to achieve high thermal efficiency. The high turbine inlet temperature requires proper cooling techniques to protect the components of the gas turbines, particularly combustor walls and turbine blades. Therefore, various cooling methods, such as film cooling, jet impingement cooling, and convective internal passage cooling, have been developed. In recent years, complex cooling techniques that are the combined forms of different cooling methods have been investigated and developed, and an impingement/effusion cooling technique is one of these combined cooling techniques.

Impingement/effusion cooling is the method that combines a full coverage film cooling (effusion cooling) and a jet impingement cooling. Full coverage film cooling is a good method to protect the surface of components from a hot gas stream and can be applied to gas turbine combustors efficiently. Jet impingement cooling is an effective way to cool the surface with locally high transfer rates. The surface heat transfer patterns can be controlled by the configuration of jet arrays. Better cooling performance can be obtained by proper combination of these cooling techniques.

Many studies of each cooling technique (array jet impingement cooling or film cooling) have been performed extensively. For the full coverage film cooling techniques, Andrews and Mkpadi,[1] Andrews et al.,[2,3] and Andrews and Bazdini Tehrani[4] investigated extensively the average heat transfer rates for full coverage film cooling with various conditions, such as hole-to-hole pitches and hole diameters. The previous studies of the jet impingement cooling technique with various parameters are well reviewed by Downs and James,[5] Jambunathan et al.,[6] and Viskanta.[7] However, there are only a few studies of the impingement/effusion cooling technique, especially for local heat transfer measurements on the inner surface of effusion plate.

Sparrow and Ortiz[8] measured average heat/mass transfer coefficients and conducted flow visualization on the upstream-facing surface of a single perforated plate (effusion only). Holes in the plate were in an equilateral hexagonal configuration, and the Reynolds number based on the hole diameter was tested between $2 \times 10^3$ and $2 \times 10^4$. The results show that the Sherwood number increases linearly with the Reynolds number.

Huber and Viskanta[9] examined the effect of spent air exit in the orifice plate on the local and average heat transfer for array of impinging jets. Their results show that the interaction of adjacent impinged jets and the flow reentrainment are reduced by the spent air exit, and then the heat transfer on target plate is enhanced.

Al Dabagh et al.[10] and Andrews and Nazari[11] investigated the effects of the number of holes on the cooling effectiveness on the outer surface of the effusion plate in the impingement/effusion cooling and reported that the influence of the number of impingement holes is small on the outer surface, but the influence of reducing the number of effusion holes is significant.

Hollworth and Dagan[12] and Hollworth and Lehmann[13] measured the average and local heat transfer coefficients of arrays of turbulent

Received 13 February 2002; revision received 22 July 2002; accepted for publication 29 July 2002. 

*Graduate Student, Department of Mechanical Engineering.
†Associate Professor, Department of Mechanical Engineering; hhcho@yonsei.ac.kr.

air jets impinging on perforated target surfaces and reported that the arrays with staggered effusion holes yield consistently higher heat transfer rates than do the impinging jets only on the solid plates.

Funazaki et al.[14] studied the heat transfer characteristics for the impingement/effusion cooling with pin fins of staggered arrangement and reported that high heat transfer is generated not only on the target plate but also on the surfaces of the pins and that high cooling performance can be obtained with less cooling air consumption.

Cho and Goldstein[15] conducted heat/mass transfer measurements on two perforated plates with a small hole-to-hole pitch, $3D$. They reported that the heat/mass transfer rates on the target surface of the second plate are approximately $45 \sim 55\%$ higher than that for the impingement cooling alone and are about three or four times that for the effusion alone (single layer).

Cho and Rhee[16] investigated the local heat/mass transfer characteristics on the inner surface of effusion plate for the impingement/effusion cooling for various gap distances and hole arrangements and reported that the cooling performance is enhanced with the small gap distance and that the injection to effusion hole arrangement is very important to obtain a high and uniform transfer on the effusion plate.

Most studies for the impingement/effusion cooling focused on the average heat transfer characteristics or overall cooling performance with the limited experimental conditions. However, a complete analysis of heat transfer with cooling techniques such as film cooling and impingement/effusion cooling requires detailed heat transfer coefficient distributions on the internal walls as well as inside the hole surfaces and adiabatic wall temperatures (film cooling effectiveness) and heat transfer coefficient distributions on the exposed surfaces.[17] In addition, information not only of overall heat transfer coefficient but also of local variation is required to prevent hot spots and to obtain better cooling design.[18] Local data are also useful to model the numerical computation and to evaluate thermal stress in this cooling system.

Therefore, in the present study, the local heat/mass transfer characteristics on the inner surface of the effusion plate are investigated with various injection hole arrangements and gap distances. Two parallel plates with circular holes are used to simulate the impingement/effusion cooling system. Three injection hole arrangements of staggered, square, and hexagonal patterns are tested with various gap distances from $1D$ to $6D$ at fixed mass flow rate through the effusion holes at the injection to effusion hole diameter ratio ($d/D$) of 0.67.

A naphthalene sublimation method is employed to measure the detailed local heat/mass transfer coefficients on the inner surface of effusion plate. One of the great advantages of this technique is accurate and easy imposition of boundary conditions analogous to isothermal or adiabatic wall in convective heat transfer without conductive and radiative losses.[19] Measured mass transfer coefficients can be converted into heat transfer coefficients using the heat and mass transfer analogy.[20]

## Experimental Apparatus and Procedure

### Experimental Apparatus

Figure 1 is a schematic view of the experimental apparatus. Room air is drawn into the settling baffle by a suction-type blower and passes through perforated plates and an orifice flow meter and then is discharged outside. Cho and Goldstein[21] reported that heat/mass transfer characteristics on the inside surface of the effusion plate are not affected by the outside crossflow (mainstream); therefore, the effect of crossflow is not considered in the present study. The injection and effusion plates are placed in a parallel position, and the various hole arrangements are achieved by changing the injection plates. T-type thermocouples are installed in a settling baffle, a plenum chamber, and the test plate to measure the accurate temperature of naphthalene surface and incoming flow.

Figures 1b and 1c are schematic views of effusion plates of the square and hexagonal hole arrangements. The naphthalene-coated test plate is placed at the center of effusion plate, which is mounted on the plenum chamber with the cross-sectional area of

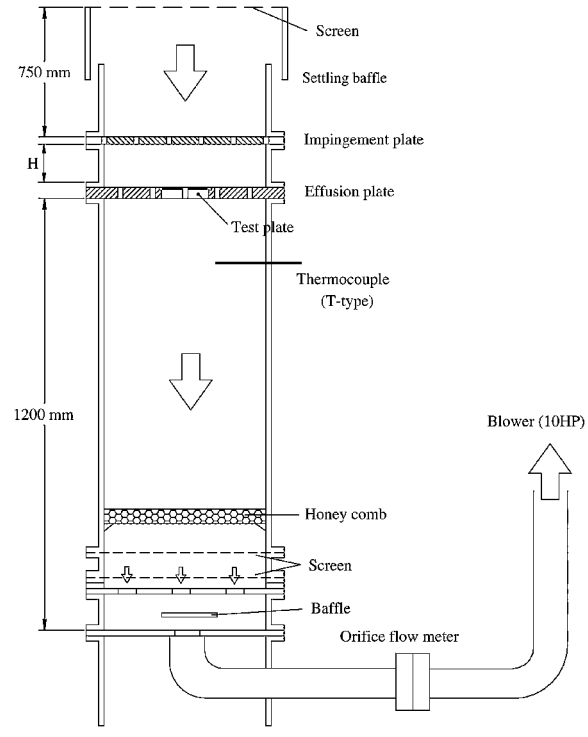


a) Test apparatus

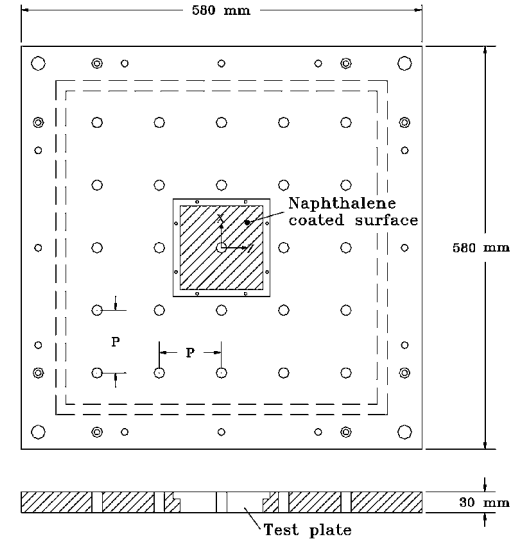


b) Effusion plate for staggered and square arrays

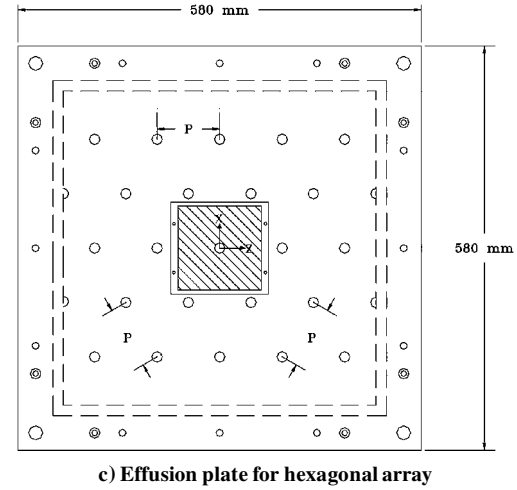


c) Effusion plate for hexagonal array

**Fig. 1 Schematic diagrams of experimental apparatus and effusion plates.**

**Table 1 Experimental parameters**

| Hole arrangement | $d$, mm | $D$, mm | Ratio of number of holes ($N_d$:$N_D$) | $A_e/A_i$ | $H/D$ | $Re_D$ | $Re_d$ |
|---|---|---|---|---|---|---|---|
| Staggered array | 10 | 15 | 1:1 (25:25) | 2.25 | 1.0, 2.0, 4.0, 6.0 | $1 \times 10^4$ | $1.5 \times 10^4$ |
| Square array | 10 | 15 | 3:1 (75:25) | 0.75 | 1.0, 2.0, 4.0, 6.0 | $1 \times 10^4$ | $5 \times 10^3$ |
| Hexagonal array | 10 | 15 | 2.4:1 (60:25) | 1.125 | 1.0, 2.0, 4.0, 6.0 | $1 \times 10^4$ | $7.5 \times 10^3$ |

$450 \times 450$ mm. The two effusion plates have 25 ($5 \times 5$) holes with pitch-to-diameter ratio ($P/D$) of 6, and the effusion hole diameter $D$ is 15 mm. The test plate has an effusion hole in the middle with the naphthalene-coated area of $8.3D \times 8.3D$. The central position of the test plate on the effusion plate with a sufficiently large number of holes ensures that endwall effects are negligible at the measuring domain. The Reynolds number based on the effusion hole diameter is fixed for $Re_D = 1 \times 10^4$ to maintain constant velocity (mass flow rate) through the effusion holes.

Schematic diagrams of hole arrangements and coordinate systems are presented in Fig. 2. Three different hole arrays are investigated for the two perforated plates: 1) staggered array with the same number of impingement holes and effusion holes (1:1) (Fig. 2a), 2) square array with the hole number ratio of 3:1 (Fig. 2b), and 3) hexagonal array with the hole number ratio of 2.4:1 (Fig. 2c). For the hexagonal hole arrangement, each injection hole locates on the gravitational center of an equilateral triangle formed by adjacent three effusion holes. These three hole arrangements are selected to investigate heat transfer distributions affected by the different flow patterns, the staggered, square, and hexagonal array jet patterns.

In general, it is desirable to design for the larger pressure drop across the injection plate (to maximize jet intensity and convective heat transfer rates), and the smaller pressure drop across the effusion plate produces lower jet velocities in film cooling situations, in turn resulting in lower boundary layer jet mixing action and better film cooling performance. Therefore, in the present study, the diameter of the injection hole is designed to be smaller than that of the effusion hole. The diameter of injection hole $d$ is 10 mm ($d/D = 0.67$) for all of the tested plates, and the thickness of the plates is $1.33D$ ($2d$).

The effusion to injection hole area ratios ($A_e/A_i$) of the staggered, square, and hexagonal arrays are 2.25, 0.75, and 1.125, respectively, because the number of injection holes is different. For all the hole arrangements, the experiments have been performed with four different gap distances $H$ of 1, 2, 4, and $6D$. The details of test parameters and operating conditions are listed in Table 1.

The results obtained in this study are compared with the results of previous work,[16] which investigated a staggered array with injection hole diameter of $d = 15$ mm to evaluate effects of the injection hole size with a fixed flow rate.

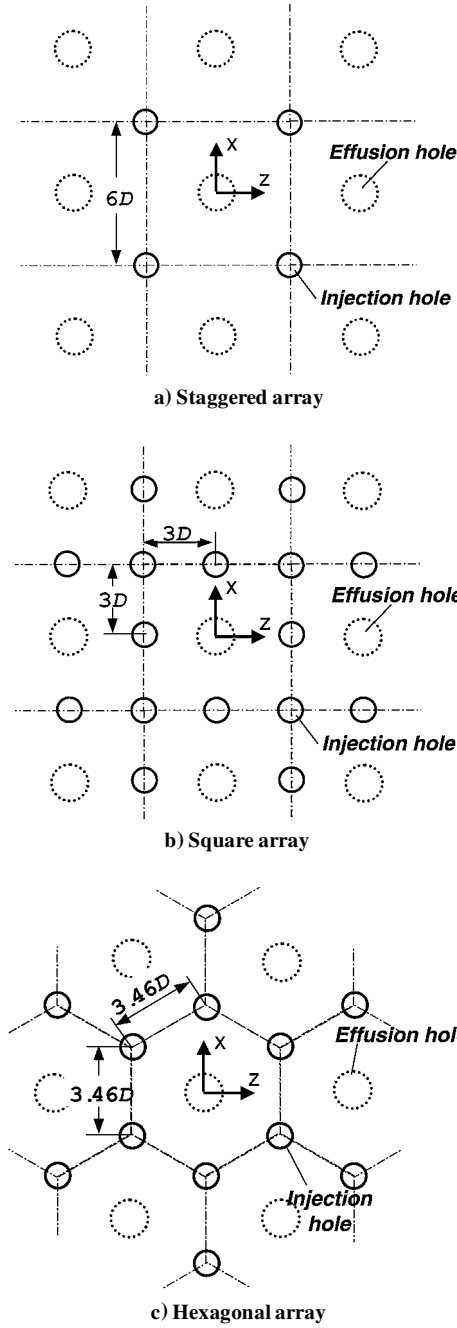


**Fig. 2 Schematic diagrams of hole arrangements.**

### Heat/Mass Transfer Coefficient

The local mass transfer coefficient is defined as

$$h_m = \frac{\dot{m}}{\rho_{v,w} - \rho_{v,\infty}} = \frac{\rho_s(\mathrm{d}y/\mathrm{d}\tau)}{\rho_{v,w}} \tag{1}$$

because the impinging jet flow contains no naphthalene, $\rho_{v,\infty} = 0$, in the present study. Therefore, the mass transfer coefficient is calculated from the local sublimation depth of naphthalene, $\mathrm{d}y$, the run time $\mathrm{d}\tau$, the density of solid naphthalene $\rho_s$, and naphthalene vapor density $\rho_{v,w}$. The naphthalene vapor density $\rho_{v,w}$ is calculated from the perfect gas law, and the naphthalene vapor pressure is obtained from a correlation of Ambrose et al.[22]

The Sherwood number can be expressed as

$$Sh = h_m D/K_{\text{naph}} \tag{2}$$

$K_{\text{naph}}$ is based on the discussion of naphthalene properties given by Goldstein and Cho.[19]

In this study, the nondimensional numbers, such as the Sherwood number, use the effusion hole diameter as a characteristic length. The heat/mass transfer of impinging jet is usually characterized by the injection hole diameter. However, the operating conditions, such as mass flow rate through the effusion holes and gap distance, are based on the effusion hole diameter in this study. Therefore, the heat/mass transfer characteristics are normalized with the effusion hole diameter in the present study.

To obtain local mass transfer coefficients $h_m$, the profile of the naphthalene surface coated on the test plate is scanned by an automated surface measuring system before and after exposure to airflow. Sublimation depth during the experiment is calculated from

the difference of the surface profiles. The measuring system consists of a depth gauge, a linear signal conditioner (Lucas ATA-101), a digital multimeter (Keithley Model 2001), two stepping-motor-driven positioners, a motor controller, and a personal computer with GPIB (Institute of Electrical and Electronics Engineering-488) board. The depth gauge is a linear variable differential transformer (LVDT) made by Schaevitz Engineering (Model LBB-375TA-020), which has a resolution of 0.025 $\mu$m. Error of the LVDT measurements on a flat plate is 0.7% of an averaged sublimation depth of 40 $\mu$m during the run. The automated system typically obtains more than 2000 data points in an hour.

The mass transfer coefficients can be converted to the heat transfer coefficients using the heat and mass transfer analogy.[20] The Prandtl number is 0.71 for air and the Schmidt number is 2.28 for the naphthalene vapor in air at 25°C. The experiments are conducted at room temperature, and the Lewis number ($Pr/Sc$) for this study is about 0.307:

$$Nu/Sh = (Pr/Sc)^{0.4}, \qquad Nu = 0.624Sh \tag{3}$$

Uncertainty of the Sherwood numbers using Kline and McClintock's[23] method for single-sample experiments, when the measured temperature, depth, position, and correlation equations are considered, is within $\pm 7.1\%$ in the entire operating range of the measurement, based on a 95% confidence interval. This uncertainty is attributed mainly to the uncertainty of properties of naphthalene, such as the naphthalene saturated vapor pressure (3.8%), and diffusion coefficient of naphthalene vapor in the air (5.1%). However, the uncertainty due to the sublimation depth measurement is only 0.7%. The other uncertainties are 0.2, 1.1, and 4.9% for $T_w$, $\rho_s$, and $h_m$, respectively.

## Results and Discussion

### Heat/Mass Transfer in Staggered Hole Arrangement

Figure 3 shows contour plots of heat/mass transfer in the staggered array for various gap distances at $Re_D = 1 \times 10^4$. The broken circles and concentric half-circles represent the projected position of the injection holes on the effusion plate and a rim of effusion hole, respectively. The experimental results show almost perfect symmetry, and so the results in the right half-regions ($0.0 \le z/D \le 3.0$) are presented in the contour plots.

As shown in Fig. 3, all of the cases show the same trend: high transfer regions are apparent near the stagnation points, whereas relatively low transfer regions are observed near the effusion hole and at the wall jet regions due to development of the boundary layer of the wall jet after impingement.

As the flow goes, the adjacent wall jets collide with each other at the midline ($z/D = 0.0$ and $x/D = 0.0$). Therefore, the upward primary vortices are formed with the countervortices impinging on the midline.[16] The countervortices enhance heat/mass transfer rates along the midline forming an additional peak (Fig. 3). Figure 4 presents the schematic view of the flow pattern on the centerplane of impinging jets. The primary vortices are formed due to the interaction of adjacent wall jets, and the counter-rotating secondary vortices are formed between the primary vortices. Therefore, the relatively low transfer regions are formed between the primary and secondary vortices, and the small peak regions are formed at the midway region due to impingement of the secondary vortices. This pattern will be shown clearly in local Sherwood number distributions (Fig. 5). The secondary vortices generated at the midway regions then flow toward the effusion holes due to the flow suction of effusion holes.

As the gap distance increases, the annular peak regions around the stagnation region disappear, as shown in Figs. 3a–3d. These heat/mass transfer patterns are related to development of the injected jets for different gap distances. The developed jet with the large gap distances produces only one peak at the stagnation point (Fig. 3d).

The local heat/mass transfer coefficients are replotted along the lines of $z/D = 3.0$ and 0.0 in Fig. 5. The points with Sherwood number value of 0 stand for the centerline of the effusion hole. With the small $H/D$ (=1.0 and 2.0), there are two peaks near the stagnation points. The inner peak, which is about $0.3D$ ($0.45d$) apart from the stagnation point, is caused by the flow acceleration that makes the boundary layer thin. The mass transfer decreases after this peak due to development of the boundary layer with decelerating flow. The boundary layer transits to turbulent flow at $x/D \cong \pm 2.2$, and the heat/mass transfer coefficient reaches a secondary peak value at

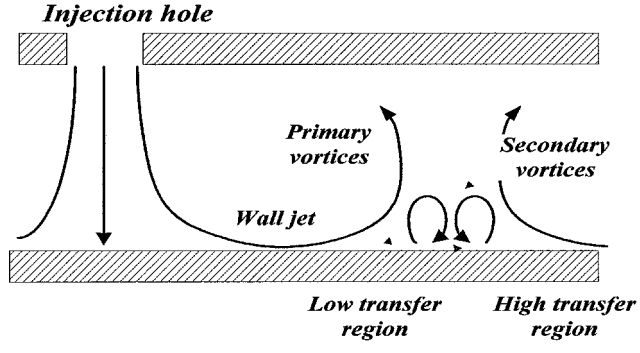


**Fig. 4 Schematic flow pattern on the centerplane of impinging jets.**

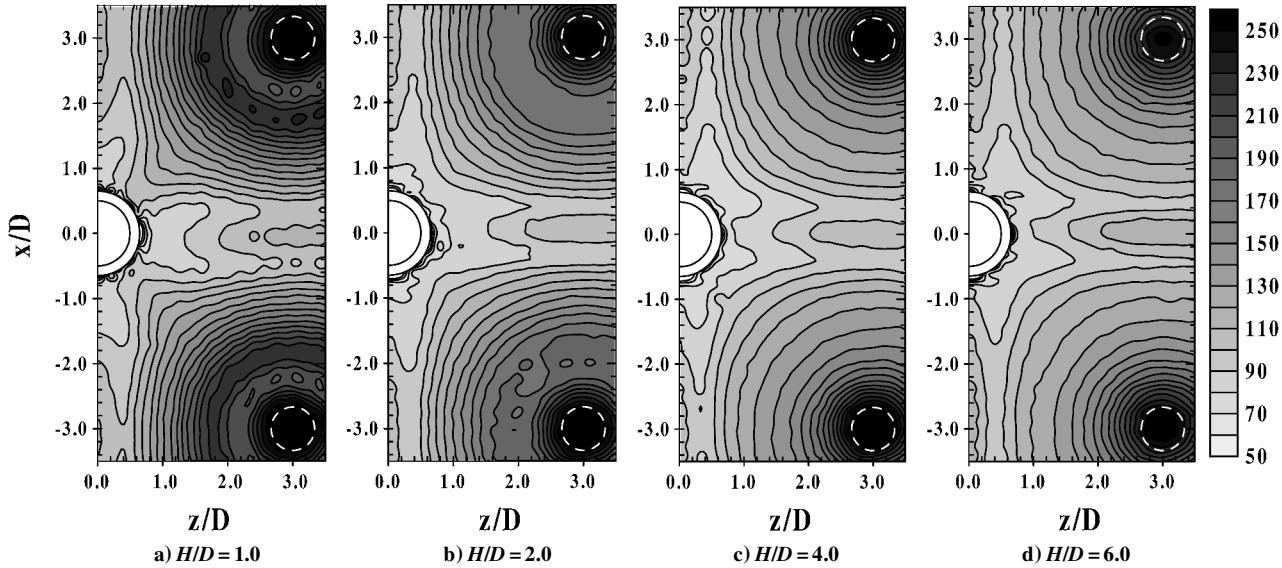


**Fig. 3 Contour plots of staggered array with $d$ = 10 mm for various gap distances.**

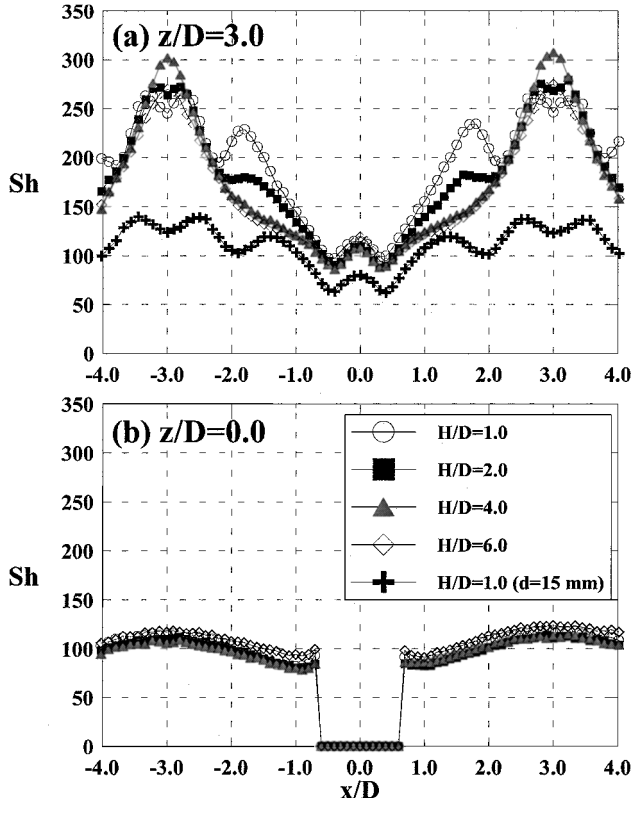


**Fig. 5 Local Sherwood number of staggered array with $d = 10$ mm for various gap distances.**

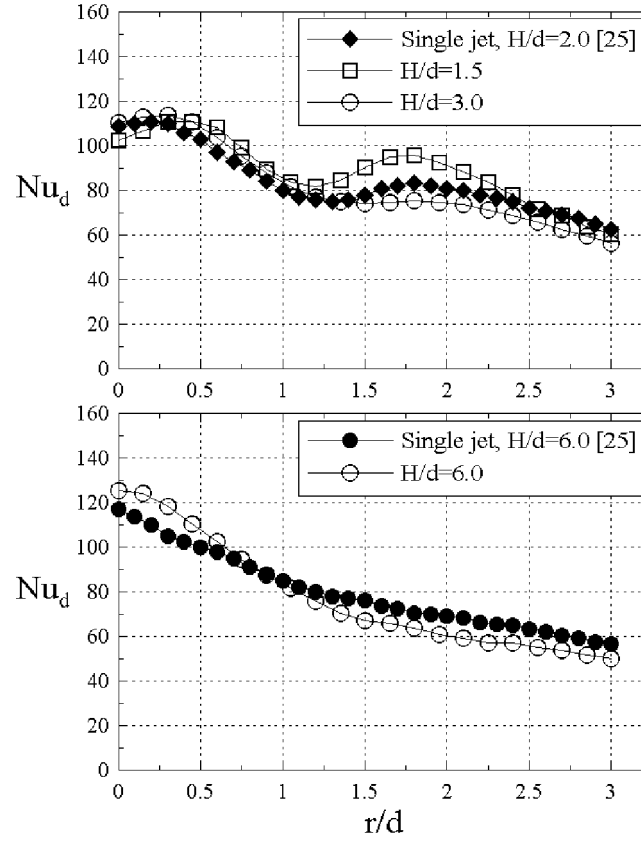


**Fig. 6 Comparison of local Nusselt number for impinging jet with other results at $Re_d = 1.5 \times 10^4$.**

the region that is approximately $1.2D$ ($1.8d$) apart from the stagnation point. This phenomenon is also referred as the secondary vortex formation. The secondary vortex is induced by unsteady flow separation, which is initiated by the unsteady adverse pressure gradient produced by the main rolling vortex.[24] The vortices on the wall disturb the boundary-layer flow and entrain the ambient fluid into the boundary layer. The secondary peak value increases with decreasing the gap distance.

With the large $H/D$ ($\geq$4.0), the turbulence intensity at the jet core increases, so that the heat/mass transfer near the stagnation point is higher than the earlier cases. However, the secondary peak disappears with the large gap distance because the flow acceleration and transition to turbulent flow are not generated with the large nozzle-to-plate distance. Thus, the local distribution of Sherwood number presents a continuously decreasing pattern. At $H/D = 4.0$ ($H/d = 6.0$, $d = 10$ mm), the heat/mass transfer coefficient of the stagnation point reaches a maximum value because the jet potential core grows to a maximum turbulence intensity before impingement on the target surface. This case is equivalent to the gap distance of six times the injection hole diameter ($H/d = 6.0$, $d = 10$ mm) and is in good agreement with results of $H/d = 6.0$ ($d = 15$ mm) in previous work.[16] At the midway region ($x/D = 0.0$), the additional peaks are observed as already mentioned. The levels of Sherwood number in the midway region are almost the same for all of the tested cases. Therefore, one can say that the strength of the secondary vortices is affected little by the gap distance between two plates.

A comparison of the results of staggered arrays with $d = 15$ and 10 mm demonstrates that the maximum and secondary peak values of the case with $d = 10$ mm are almost twice those with $d = 15$ mm (Fig. 5a). It is because the air jet through injection hole of $d = 10$ mm has much higher momentum than that of $d = 15$ mm for the same Reynolds number $Re_D$ (the same mass flow rate). Although each case has large differences in local values, both cases show the similar heat/mass transfer patterns.

Figure 6 presents the local Nusselt number distributions obtained by the heat/mass transfer analogy [Eq. (3)] of the present study ($H/d = 1.5$ and 3.0) and another single jet result[25] ($H/d = 2.0$) for $Re_d = 1.5 \times 10^4$. For the small gap distances, the distributions are in accordance with the single jet result. For the large gap distance of $H/d = 6.0$, some discrepancies are observed in stagnation and wall jet regions. This is possibly due to the differences in the experimental conditions. For example, for the single jet, the fully developed pipe jet impinges on the target plate, whereas the array jets are injected through the injection plate (nozzle plate) in this study.

#### Heat/Mass Transfer in Square Hole Arrangement

Figure 7 presents the contour plots of the Sherwood number for the square hole arrangement with various gap distances. Although more uniform heat/mass transfer distributions are obtained due to the increase of number of the injection holes, the overall levels of Sherwood number are much lower than those for the staggered arrangement due to the decrease of the injected jet velocity. In addition, locally low transfer regions are formed at $x/D = \pm 1.5$ and $z/D = 1.5$, especially for the large gap distance ($H/D = 6.0$). The reason is that the distance between centers of injection and effusion holes is longer, and then the strength of the wall jet of the far-off impinging jet ($x/D = \pm 3.0$ and $z/D = 3.0$) is weak. The regions of weak transfer rates widen, and the levels of Sherwood number decrease as the gap distance increases. These locally low transfer regions should be avoided to prevent hot spots on a component.

Figure 8 presents the local distributions of the Sherwood number. Along the line of $z/D = 3.0$, the graph includes three stagnation points of impinging jets. This means that the hole-to-hole pitch of the impingement jets is reduced to half ($3D$) of that of the staggered arrangement, whereas the pitch of the impinging jets at $z/D = 0.0$ is the same as the case of staggered array ($6D$) as shown in Fig. 2.

At $z/D = 3.0$ (Fig. 8a), the adjacent wall jets collide with each other before transition of the boundary layer due to the smaller pitch, and the secondary peaks are not generated. Note that the valleys and peaks near the stagnation points are observed for the smallest gap distance of $H/D = 1.0$ due to the flow acceleration. At the

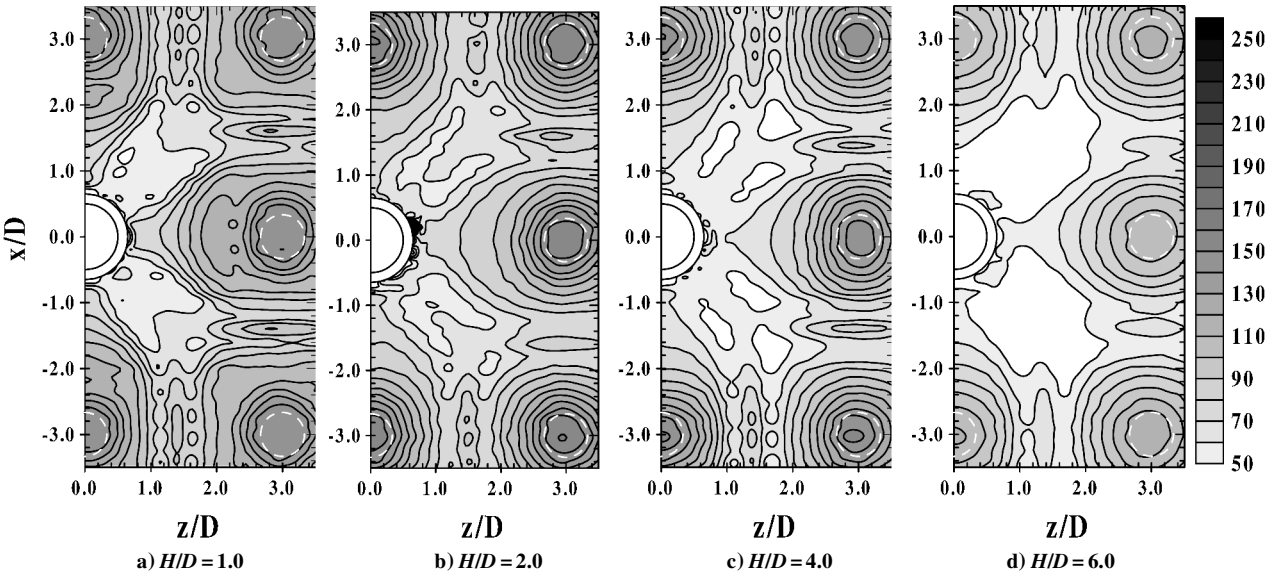


**Fig. 7 Contour plots of Sherwood number for square array with $d = 10$ mm for various gap distances.**

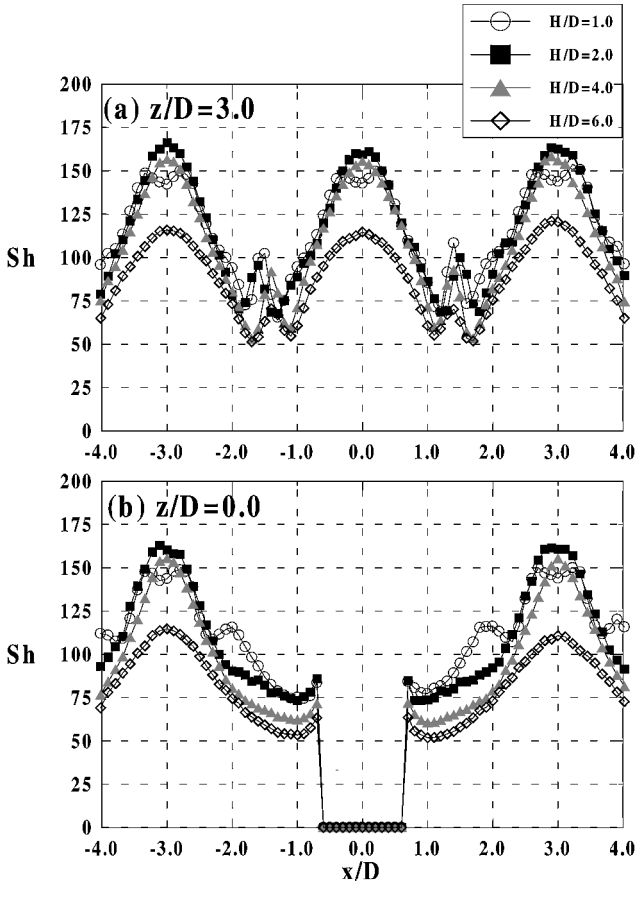


**Fig. 8 Local Sh of square array with $d = 10$ mm for various gap distances.**

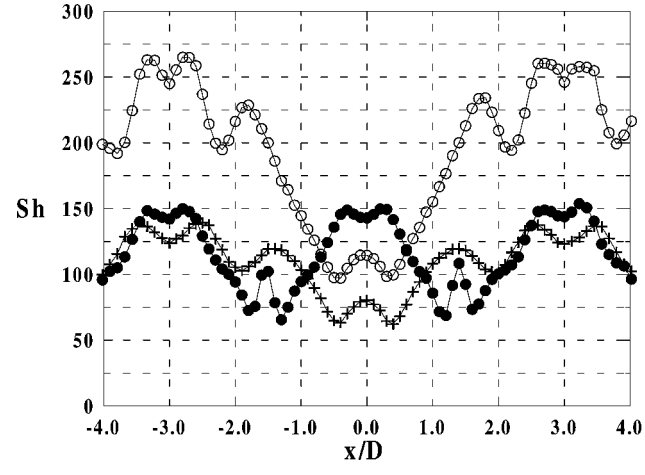


**Fig. 9 Local Sherwood number of various hole arrangements at $z/D = 3.0$ for $H/D = 1.0$: ○, staggered array ($d = 10$ mm); ●, square array ($d = 10$ mm); and +, staggered array ($d = 15$ mm).**

midway regions ($x/D = \pm 1.5$), the additional peaks are formed by the counter-rotating secondary vortices explained in Fig. 4.

The Sherwood number at the stagnation point indicates the highest value obtained with $H/D = 2.0$ ($H/d = 3.0$), whereas the highest Sherwood number is observed at $H/D = 4.0$ ($H/d = 4.0$) for the staggered hole arrangement, as shown in Fig. 5. The reason for this is that the interaction of adjacent jets is stronger than that for the staggered hole arrangement, and the jets develop more quickly due to the smaller hole-to-hole pitch. In addition, it may be that the Reynolds number based on the injection hole ($Re_d$) is smaller than that of the staggered array due to lower jet velocity, and the jet flow with smaller Reynolds number $Re_d$ is more likely to develop than that with larger Reynolds number $Re_d$.

At $z/D = 0.0$, the monotonous Sherwood number patterns from the stagnation point to effusion hole are observed for all gap distances, except for $H/D = 1.0$. For $H/D = 1.0$, the secondary peak is clearly observed at $x/D \cong 2.0$ due to the flow transition, which is hardly noticed at $z/D = 3.0$ in Fig. 8.

Figure 9 presents the effects of the number of holes on the line of $z/D = 3.0$ at $H/D = 1.0$. The peak Sherwood number values of the square array are much lower than those of the staggered array with $d = 10$ mm due to the lower injection hole velocity. However, the maximum Sherwood number of the square array is slightly higher than that of the staggered array of $d = 15$ mm in spite of the smaller $A_e/A_i$. The reason for this is that the jet flow from the hole of $d = 10$ mm has longer distance between the plates (in terms of $H/d$) to develop, so that the flow gains higher turbulence intensity than that from the hole of $d = 15$ mm for the same gap distance due to the stronger interaction between the adjacent jets. In addition, there is another stagnation point at $x/D = 0.0$ for the square arrangement, and more uniform distribution is clearly achieved. However, the locally low transfer regions are formed with the square hole arrangement as shown in Fig. 7 due to its geometric

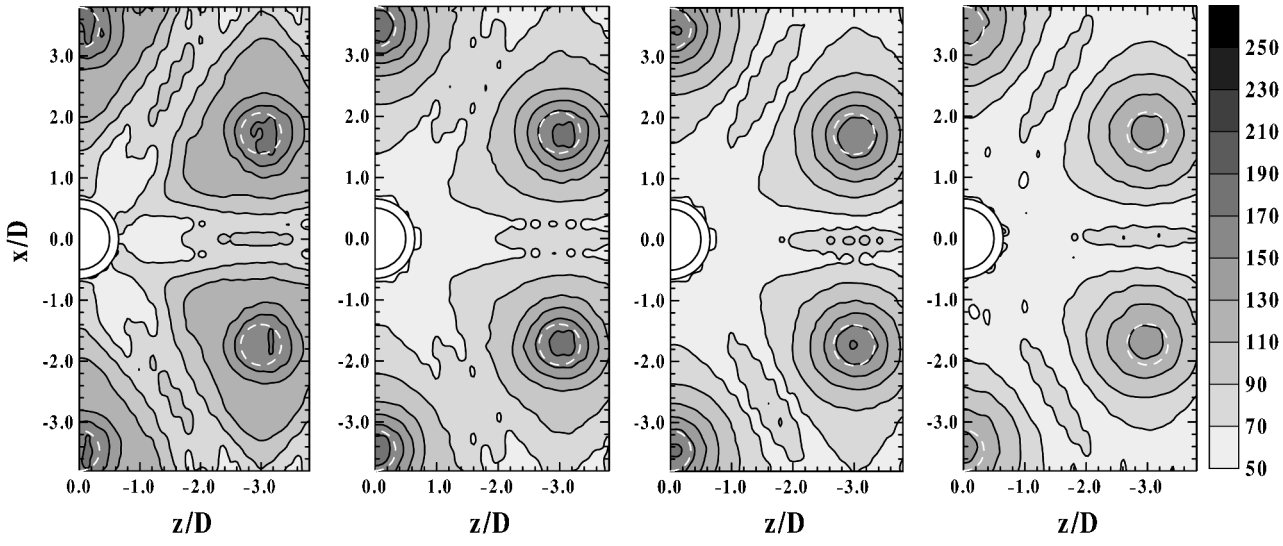


a) $H/D = 1.0$ b) $H/D = 2.0$ c) $H/D = 4.0$ d) $H/D = 6.0$

**Fig. 10 Contour plots of Sherwood number for hexagonal array with $H/D = 1.0$ at $Re_D = 1 \times 10^4$.**

feature, and the existence of low transfer regions is not desirable in the hot-temperature components as mentioned before.

### Heat/Mass Transfer in Hexagonal Hole Arrangement

Figure 10 shows the contour plots of the Sherwood number for the hexagonal array at $Re_D = 1 \times 10^4$. The injection hole is located on the gravitational center of an equilateral triangle formed by adjacent three effusion holes. Therefore, the wall jet flow after impingement on the target plate is divided into three directional flows, and each of those goes into one of the three effusion holes that are in the same distances from the stagnation point. This flow pattern makes the dark region (relatively high transfer region) that has an equilateral triangular pattern in the contour.

The overall Sherwood number decreases as $H/D$ increases, and it is the same trend as with the staggered and square hole arrangements. However, even at the large gap distances, the Sherwood number contour shows fairly uniform distributions with little low transfer regions between the impingement jets.

Figure 11 presents the local distributions of Sherwood number for the hexagonal arrangement. The Sherwood values at the stagnation points are about 10% higher than those for the square arrangement because the area ratio of effusion to injection hole is increased. For the small gap distance of $H/D = 1.0$, the secondary peaks due to the flow transition are observed clearly. However, for $H/D \geq 2.0$, the overall heat/mass transfer decreases as the gap distance increases. Especially, the heat/mass transfer at the wall jet regions decreases significantly. However, as already mentioned, the uniform heat/mass transfer distributions are obtained with the hexagonal hole arrangements without the low transfer regions (hot spots).

### Average Heat/Mass Transfer

Figure 12 presents the average Sherwood numbers for various hole arrangements at $Re_D = 1 \times 10^4$. For the staggered and square hole arrangements, the average values are obtained by numerical integration on the region of $-3.0 \leq x/D \leq 3.0$ and $0.0 \leq z/D \leq 3.0$. The average values for the hexagonal array are obtained on the triangular region formed by centers of the effusion hole and two adjacent injection holes.

For all tested cases, the average Sherwood numbers indicate the maximum values at $H/D = 1.0$ (the smallest gap distance in the present study) and decrease continuously as the gap distance increases. Average Sherwood number $\overline{Sh}$ for the staggered arrangement of $d = 10$ mm is the highest for all gap distances because of the high jet flow velocity. As expected from the local distributions of Sherwood number, the average values for the square arrangement

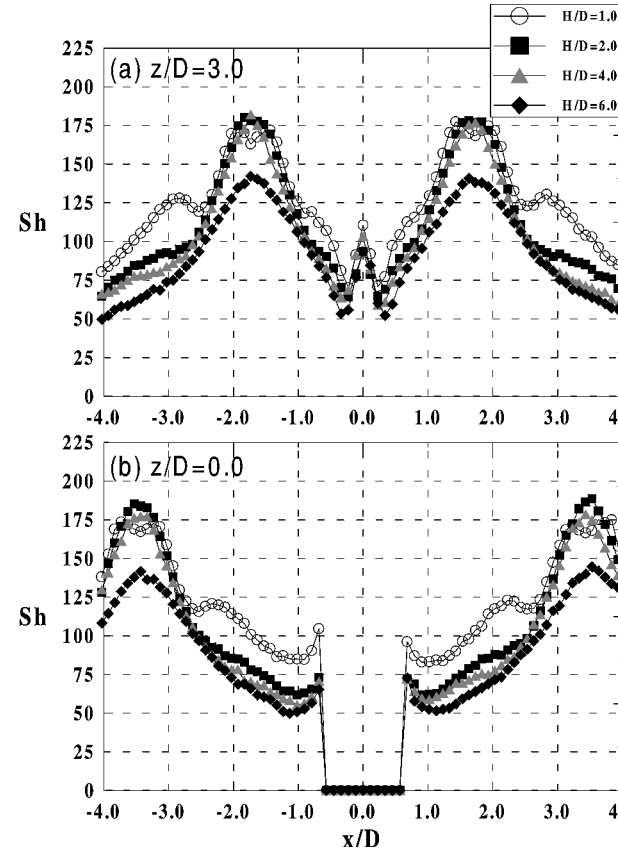


**Fig. 11 Local plots of Sherwood number for hexagonal array with $H/D = 1.0$ at $Re_D = 1 \times 10^4$.**

are about 10% lower than those for the hexagonal arrangement and the staggered hole arrangement of $d = 15$ mm due to the decreased area ratio ($A_e/A_i$).

For the hexagonal hole arrangement, the average values are almost the same as those for the staggered array of $d = 15$ mm because the area ratio is close to a unity and the low transfer region observed in the square array has disappeared.

Although the average Sherwood number $\overline{Sh}$ of the staggered array of $d = 10$ mm is the highest in all $H/D$, from the view points of heat transfer uniformity involving the thermal stress problem, the

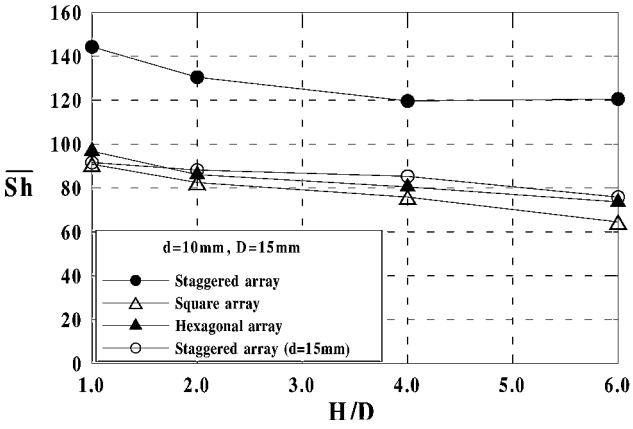


**Fig. 12 Average Sherwood number for different arrays and various gap distances at $Re_D = 1 \times 10^4$.**

hexagonal arrangements will be one choice of the impingement/effusion cooling system.

## Conclusions

In the present study, the local heat/mass transfer characteristics on the inner surface of the effusion plate are investigated with various hole arrangements and gap distances.

In the impingement/effusion cooling, the high transfer regions on the effusion plate are formed on the stagnation regions and the additional peaks are formed at the midway regions due to the interaction between the wall jets. The heat/mass transfer coefficient distributions are fairly symmetric because the spent air is discharged through the effusion holes.

For the staggered hole arrangement, the local Sherwood numbers show the highest values among all tested cases due to the high impinging jet flow velocity related to the large effusion to injection hole area ratio. However, the local distribution is very nonuniform resulting in high thermal stress in hot-temperature components.

For the square hole arrangement, although the overall levels of Sherwood number are lower than those for the staggered arrangement, relatively uniform distributions are obtained because the number of injection holes is increased. However, for relatively large gap distances, the square hole arrangement includes the locally low transfer regions (hot spots) formed near the effusion holes.

For the hexagonal hole arrangement, the equilateral triangular cells of high transfer rates are formed and fairly uniform distributions are obtained for all tested gap distances ($1.0 \leq H/D \leq 6.0$). The average Sherwood numbers are about 10% higher than those for the square arrangement due to the increase of effusion to injection hole area ratio.

The average Sherwood number decreases as the gap distance increases for all tested hole arrangements and increases with increasing area ratio of effusion to injection hole. This implies that the effusion to injection hole area ratio is a more dominant factor than the hole arrangement for the average performance estimate in the impingement/effusion cooling system.

## Acknowledgment

The authors acknowledge support for this study by Ministry of Science and Technology through National Research Laboratory program.

## References

[1]Andrews, G. E., and Mkpadi, M. C., "Full-Coverage Discrete Hole Wall Cooling: Discharge Coefficients," *Journal of Engineering for Gas Turbines and Power*, Vol. 106, No. 1, 1984, pp. 183–192.

[2]Andrews, G. E., Alikhanizadeh, M., Asere, A. A., Hussain, C. I., Khoshkabar Azari, M. S., and Mkpadi, M. C., "Small Diameter Film Cooling Holes: Wall Convective Heat Transfer," *Journal of Turbomachinery*, Vol. 108, No. 4, 1986, pp. 283–289.

[3]Andrews, G. E., Alikhanizadeh, M., Bazdini Tehrani, F., Hussain, C. I., and Khoshkabar Azari, M. S., "Small Diameter Film Cooling Holes: The Influence of Hole Size and Pitch," American Society of Mechanical Engineers, ASME Paper 87-GT-28, 1987.

[4]Andrews, G. E., and Bazdini Tehrani, F., "Small Diameter Film Cooling Hole Heat Transfer: The Influence of the Number of Holes," American Society of Mechanical Engineers, ASME Paper 89-GT-7, 1989.

[5]Downs, S. J., and James, E. H., "Jet Impingement Heat Transfer—A Literature Survey," American Society of Mechanical Engineers, ASME Paper 87-HT-35, 1987.

[6]Jambunathan, K., Lai, E., Moss, M. A., and Button, B. L., "A Review of Heat Transfer Data for Single Circular Jet Impingement," *International Journal of Heat and Fluid Flow*, Vol. 13, No. 2, 1992, pp. 106–115.

[7]Viskanta, R., "Heat Transfer to Impinging Isothermal Gas and Flame Jets," *Experimental Thermal and Fluid Science*, Vol. 6, 1993, pp. 111–134.

[8]Sparrow, E. M., and Ortiz, M. C., "Heat Transfer Coefficients for the Upstream Face of a Perforated Plate Positioned Normal to an Oncoming Flow," *International Journal of Heat and Mass Transfer*, Vol. 25, No. 1, 1982, 127–135.

[9]Huber, A. M., and Viskanta, R., "Effect of Jet–Jet Spacing on Convective Heat Transfer to Confined, Impinging Arrays of Axisymmetric Air Jets," *International Journal of Heat and Mass Transfer*, Vol. 37, No. 18, 1994, pp. 2859–2869.

[10]Al Dabagh, A. M., Andrews, G. E., Abdul Husain, R. A. A., Hussain, C. I., Nazari, A., and Wu, J., "Impingement/Effusion Cooling: The Influence of the Number of Impingement Holes and Pressure Loss on the Heat Transfer Coefficient," *Journal of Turbomachinery*, Vol. 112, No. 3, 1990, pp. 467–476.

[11]Andrews, G. E., and Nazari, A, "Impingement/Effusion Cooling: Influence of the Number of Holes on the Cooling Effectiveness for an Impingement $X/D$ of 10.5 and Effusion $X/D$ of 7.0," *Proceedings of 7th IGTC*, Vol. 2, Gas Turbine Society of Japan, Toyko, Japan, 1999, pp. 639–646.

[12]Hollwarth, B. R., and Dagan, L., "Arrays of Impinging Jets with Spent Fluid Removal through Vent Holes on the Target Surface Part 1: Average Heat Transfer," *Journal of Engineering for Power*, Vol. 102, No. 4, 1980, pp. 994–999.

[13]Hollwarth, B. R., Lehmann, G., and Rosiczkowski, J., "Arrays of Impinging Jets with Spent Fluid Removal Through Vent Holes on the Target Surface Part 2: Local Heat Transfer," *Journal of Engineering for Power*, Vol. 105, No. 2, 1983, pp. 393–402.

[14]Funazaki, K., Imamatsu, N., and Yamawaki, S., "Heat Transfer Measurements of an Integrated Cooling Configuration Designed for Ultra-High Temperature Turbine Blades," *Proceedings of 7th IGTC*, Vol. 2, Gas Turbine Society of Japan, Toyko, Japan, 1999, pp. 833–840.

[15]Cho, H. H., and Goldstein, R. J., "Effect of Hole Arrangements on Impingement/Effusion Cooling," *Proceedings of the 3rd KSME–JSME Thermal Engineering Conference*, Korean Society of Mechanical Engineers/Japanese Society of Mechanical Engineers, Seoul, Korea, 1996, pp. 71–76.

[16]Cho, H. H., and Rhee, D. H., "Local Heat/Mass Transfer Measurement on the Effusion Plate in Impingement/Effusion Cooling Systems," *Journal of Turbomachinery*, Vol. 123, No. 3, 2001, pp. 601–608.

[17]Goldstein, R. J., Cho, H. H., and Jabbari, M. Y., "Effect of Plenum Crossflow on Heat (Mass) Transfer Near and Within the Entrance of Film Cooling Holes," *Journal of Turbomachinery*, Vol. 119, No. 4, 1997, pp. 761–769.

[18]Cho, H. H., and Goldstein, R. J., "Total Coverage Discrete Hole Wall Cooling," *Journal of Turbomachinery*, Vol. 119, No. 2, 1997, pp. 320–329.

[19]Goldstein, R. J., and Cho, H. H., "A Review of Mass Transfer Measurement Using Naphthalene Sublimation," *Experimental Thermal and Fluid Science*, Vol. 10, No. 4, 1995, pp. 416–434.

[20]Eckert, E. R. G., "Analogies to Heat Transfer Processes," *Measurements in Heat Transfer*, edited by E. R. G. Eckert and R. J. Goldstein, Hemisphere, New York, 1976, pp. 397–423.

[21]Cho, H. H., and Goldstein, R. J., "Heat (Mass) Transfer and Film Cooling Effectiveness with Injection Through Discrete Holes—Part I: Within Holes and on the Back Surface," *Journal of Turbomachinery*, Vol. 117, No. 3, 1995, pp. 440–450.

[22]Ambrose, D., Lawrenson, I. J., and Sparke, C. H. S., "The Vapor Pressure of Naphthalene," *Journal of Chemical Thermodynamics*, Vol. 7, 1975, pp. 1173–1176.

[23]Kline, S. J., and McClintock, F., "Describing Uncertainty in Single Sample Experiments," *Mechanical Engineering*, Vol. 75, 1953, pp. 3–8.

[24]Cho, H. H., Lee, C. H., and Kim, Y. S., "Characteristics of Heat Transfer in Impinging Jets by Control of Vortex Pairing," American Society of Mechanical Engineers, ASME Paper 97-GT-276, 1997.

[25]Lee, J. H., and Lee, S. J., "Turbulent Heat Transfer Characteristics in a Stagnation Region of Axi-Symmetric Jet Impingement," *Proceedings of 11th IHTC*, Vol. 5, International Scientific Committee, Seoul, Korea, 1998, pp. 433–438.